APS physics

CHORUS

This is the accepted manuscript made available via CHORUS. The article has been published as:

Classical Impurity Ion Confinement in a Toroidal Magnetized Fusion Plasma

S. T. A. Kumar, D. J. Den Hartog, K. J. Caspary, R. M. Magee, V. V. Mirnov, B. E. Chapman, D. Craig, G. Fiksel, and J. S. Sarff

Phys. Rev. Lett. **108**, 125006 — Published 22 March 2012

DOI: 10.1103/PhysRevLett.108.125006

Classical impurity ion confinement in a toroidal magnetized fusion plasma

S. T. A Kumar[1,2],* D. J. Den Hartog[1,2], K. J. Caspary[1], R. M. Magee[1],† V. V. Mirnov[1,2], B. E. Chapman[1], D. Craig[3], G. Fiksel[2,4], and J. S. Sarff[1,2]

[1]*Department of Physics, University of Wisconsin-Madison, Madison, WI 53706, USA*

[2]*Center for Magnetic Self-Organization in Laboratory and Astrophysical Plasmas, University of Wisconsin-Madison, Madison, WI 53706, USA*

[3]*Wheaton College, Wheaton, IL, USA and*

[4]*Laboratory for Laser Energetics, University of Rochester, NY, USA*

Abstract

High-resolution measurements of impurity ion dynamics provide first-time evidence of classical ion confinement in a toroidal, magnetically confined plasma. The density profile evolution of fully-stripped carbon is measured in MST reversed-field pinch plasmas with reduced magnetic turbulence to assess Coulomb-collisional transport without the neoclassical enhancement from particle drift effects. The impurity density profile evolves to a hollow shape, consistent with the temperature screening mechanism of classical transport. Corroborating methane pellet injection experiments expose sensitivity of the impurity particle confinement time to the residual magnetic fluctuation amplitude.

The enhancement of classical Coulomb-collisional diffusive transport that occurs as a result of particle drifts in a toroidal, magnetically confined plasma is well-developed theoretically, and is known as neoclassical transport [1]. Experimentally, transport in toroidal magnetic fusion devices like the tokamak and stellarator is typically larger than neoclassical values due to diffusion related to plasma turbulence. However, at least for ion transport, some plasma confinement conditions with low levels of turbulence have attained neoclassical values [2–4], the theoretical lower bound in configurations with a strong toroidal magnetic field. The reversed-field pinch (RFP) magnetic configuration is unlike the tokamak and stellarator in that the gradient in $|\mathbf{B}|$ is nearly normal to the concentric toroidal magnetic surfaces, and the magnetic connection length along a field line connecting the toroidally inboard and outboard regions of a magnetic flux surface is shorter because the poloidal and toroidal components are the same order. The drift of particle guiding centers off a magnetic surface is therefore small, for example, the radial width of the banana-shaped drift orbit for particles trapped in the toroidal magnetic mirror is smaller than the particle gyro-radius. Hence, the lower limit for radial transport in the RFP is classical rather than neoclassical, even though some toroidal effects persist, such as an enhancement of the parallel electrical resistivity from particle trapping in the toroidal magnetic mirror [5–8]. The transport in RFP plasmas has typically been much larger than classical as a result of turbulence from large-scale magnetic tearing instabilities. In recent years, techniques have been developed to suppress this turbulence, yielding diffusion coefficients that are reduced locally as much as 30-fold [9–13]. This creates a unique opportunity to confirm transport from Coulomb collisions without the adverse neoclassical enhancement from toroidicity.

In this Letter we provide experimental evidence for the attainment of classical ion transport in a toroidal plasma. Measurements of the radial profile evolution of several impurity ion species, in particular C^{+6}, reveal outward convection and the development of a hollow profile of impurity density at the onset of improved confinement using inductive current profile control in the MST RFP (major radius R = 1.5 m, minor radius a = 0.52 m) [14]. This hollow profile is consistent with classical confinement expectations, resulting from the temperature screening mechanism operative when the temperature profile has a stronger gradient than the density profile. Modeling of particle diffusion shows that the timescale for the carbon profile evolution is also consistent with classical transport. Measurements of other

dominant ion species (at fewer spatial points) are included to account for ion-ion collisions. Experiments using injection of frozen methane pellets are also reported that corroborate conclusions based on the natural evolution of carbon impurity sourced from plasma-facing graphite structures mounted on the vacuum vessel. Hollow impurity ion profiles have been observed in tokamak and stellarator plasmas, depending on particular conditions of the thermal pressure gradient and collisionality[15, 16]. In general, hollow impurity profiles should be favorable for the removal of helium "ash" and other impurities in a fusion reactor plasma.

The studies reported here are made in improved-confinement MST deuterium plasmas with toroidal plasma current $\sim$ 400 kA, line-averaged central electron density $n_e \sim 0.8 - 1 \times 10^{19}$ m^{-3}, central electron temperature $\sim$1 keV and central ion temperature $\sim$ 0.4 keV. Ion gyro-radii are $<$ 1 cm. Improved confinement discharges are obtained using inductive control of tearing instability, a technique called "Pulsed Parallel Current Drive" (PPCD) [9, 10]. The main characteristics of PPCD discharges are reduced magnetic stochasticity, higher core electron temperature and improved energy and particle confinement [11, 12]. Transport in a stochastic magnetic field has been the principal confinement challenge for RFP plasmas. The test-particle diffusivity [17], $D_{st} = v_{T_i} D_m$, is reduced by more than an order of magnitude with PPCD to $D_{st} \sim 0.1$ m^2/s, where v_{T_i} is the ion thermal velocity and $D_m \approx 10^{-6}$ m is the estimated stochastic magnetic field diffusivity for the smaller magnetic fluctuations attained [18]. This value of D_{st} is below the classical transport level for ions. Time evolution of plasma parameters for a typical PPCD discharge in MST is shown in Figs.1 (a)-(d). The increase in soft-x-ray emission is mainly due to the increase in the electron temperature (typically from $\sim$ 400 eV to $\sim$ 1.2 keV during 400 kA PPCD).

The density of C^{+6} is measured using a fast, active charge-exchange-recombination-spectroscopy diagnostic with high spatial ($\sim$ 2 cm) and temporal (up to 10 μs) resolution [19–21]. This entails the collection of C VI emission at λ = 343.4 nm (n=7 to n=6 transition) which is stimulated by charge exchange between C^{+6} ions and a beam of 50 keV hydrogen atoms injected radially. The local impurity density (n_z) is calculated from the charge-exchange emission brightness [22].

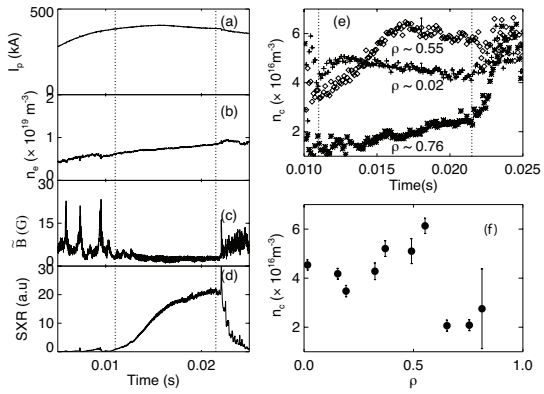

FIG. 1. (a-d) Time evolution of a typical PPCD discharge. (a) Plasma current, (b) line-averaged electron density, (c) mean amplitude of core-resonant magnetic fluctuations ($\sqrt{\sum_{m,n} \tilde{B}_{\theta}{}^{2}_{m,n}}$, m=1, n=7-12 modes), and (d) soft-x-ray emission. The dotted vertical lines indicate the duration of the PPCD improved confinement period. (e) Evolution of C^{+6} density at three radial locations, and (f) the nearly stationary C^{+6} radial profile towards the end of PPCD. Data shown in (e) and (f) are averaged over similar discharges. Error bars represent standard deviation of the mean.

The temporal behavior of the C^{+6} density at three minor radial locations ($\rho = r/a \sim$ 0.02, 0.55 and 0.76) are plotted in Fig.1(e). A slow decay of the fully-stripped carbon density in the core ($\rho \sim 0.02$) is apparent during the improved confinement period, following an initial transient increase that reflects residual ionization as the electron temperature rapidly increases. The impurity density in the outer region of the plasma, on the other hand, is slowly increasing. The profile in the core region ($0 \leq \rho \leq 0.6$) approaches a stationary hollow shape toward the end of PPCD. The radial profile of C^{+6} density averaged over ~ 2 ms toward the end of PPCD is shown in Fig.1(f) and shows the hollow radial profile.

Our calculations of impurity ionization balance using ADAS [23] (without transport) show that, in PPCD discharges, due to the high electron temperature, light impurities are mostly fully stripped, and the source (lower charge states) is small in most of the plasma volume. This result is supported by the experimental observation of a slow decay in the core impurity density, even though the core electron temperature is increasing during PPCD. The slow decay of the impurity density in the core region concurrent with the increase in impurity density in the outer region hence implies an outward convection of impurities. The slow increase of impurity density in the far-outer region ($\rho \geq 0.7$) is, however, attributed

partly to the increasing ionization due to increasing electron temperature.

The classical radial impurity flux (Γ_c) due to Coulomb collisions with the main ions is given by [24]

$$\Gamma_c = \frac{\nu_i \rho_i^2 n_i}{2Z}\left[\frac{\partial \ln P_i}{\partial r} - \frac{T_c \partial \ln P_c}{T_i Z \partial r} - \frac{3\partial \ln T_i}{2\partial r}\right] \tag{1}$$

for $m_c >> m_i$, where subscripts c & i represent impurity and main ions, m, P, T, ρ, ν and Z are, respectively, the ion mass, pressure, temperature, gyro radius, collision frequency and atomic number. The steady-state impurity radial density profile, obtained by setting the radial flux equal to zero, is $\frac{n_c(r)}{n_c(0)} = \left[\frac{n_i(r)}{n_i(0)}\right]^Z \left[\frac{T_i(r)}{T_i(0)}\right]^{\frac{-Z}{2}-1}$, where equilibration of temperatures, $T_c = T_i$, is assumed. It can be seen that the density and temperature gradients of the main ions act in opposite ways: a negative density gradient leads to core impurity accumulation, while a negative temperature gradient leads to impurity expulsion. This effect is generally called the "temperature screening," where the thermal force due to the ion temperature gradient expels impurities from the plasma core. As the ion density profile is nearly flat in the plasma core, and because there exists a strong ion temperature gradient, classical transport analysis predicts a hollow impurity ion density profile for PPCD discharges. Temperature screening and a hollow impurity profile have been observed in the tokamak in the past [15]. This, however, requires both the main and impurity ions to be in the long-mean free path regime. A tokamak plasma with parameters similar to those in MST would have collisionality in the "plateau" regime of neoclassical transport, and the sign of the temperature gradient term would be opposite, leading instead to impurity profile peaking [25].

Equation (1) provides the flux of impurity ions due to collisions with the main light ions only. Collisions with other impurities could significantly modify carbon transport. For example, the mechanism of temperature screening is mass dependent, such that collisions with higher mass impurities could lead to impurity accumulation instead of impurity expulsion. Analysis for multiple impurity ion species yields [26]

$$\Gamma_c = n_c \rho_c^2 \sum_\beta \left(\frac{m_\beta}{m_c + m_\beta}\right)^{1/2} \nu_{c\beta}\left[-\nabla \ln p_c + \frac{Z_c}{Z_\beta}\nabla \ln p_\beta + \frac{3}{2}\frac{m_\beta}{m_\beta + m_c}\left(1 - \frac{m_c Z_c}{m_\beta Z_\beta}\right)\nabla \ln T\right] \tag{2}$$

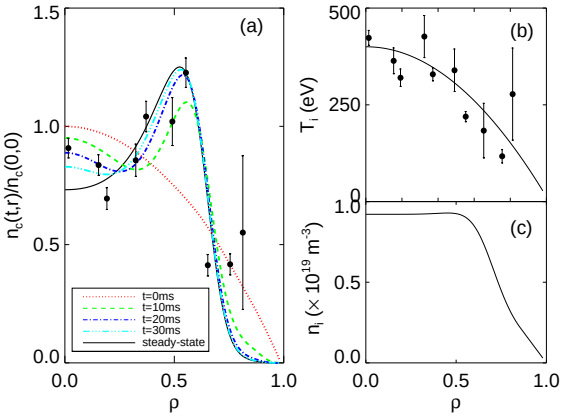

FIG. 2. (a) Time evolution of carbon profile predicted by the classical model. An initial parabolic profile (dotted line) evolves to the steady-state profile (solid line) in ≈ 40 ms. Experimental C^{+6} density profile (closed circles), scaled for best fit, is also plotted for comparison. (b) Measured C^{+6} temperature (closed circles) and the ion temperature profile used in the model (solid line). (c) The main ion density (n_i) profile used in the model, calculated from n_e and impurity density profiles, assuming charge neutrality.

where $\nu_{c\beta} = \frac{16\pi^{1/2}}{2^{3/2}3} n_\beta \ln\Lambda \left(\frac{T}{m_c}\right)^{1/2} \left(\frac{Z_c Z_\beta e^2}{4\pi\epsilon_0 T}\right)^2$ is the collision frequency of carbon with deuterons and other identified dominant impurity ions (boron, oxygen and aluminum) in MST. Densities of B^{+5}, O^{+8}, Al^{+11} and Al^{+13} ions are measured using charge-exchange-recombination-spectroscopy in similar discharges [22, 27]. All impurities and main ions are assumed to have the same temperature profile, as the impurity-main-ion energy equilibration time ($\sim$ 0.1 ms) is much less than the impurity life-time ($\sim$ 30-40 ms). This is consistent with majority and impurity ion temperature measurements to date [13].

To interpret the impurity density measurements, the spatial and temporal evolution of the carbon density is modeled for a given initial radial profile using the diffusion equations, $\frac{\partial n_c}{\partial t} = -\frac{1}{r}\frac{\partial(r\Gamma_c)}{\partial r} + S$ and $\Gamma_c = -D(r)\frac{\partial n_c}{\partial r} + V(r)n_c$, where S is the source term, D is the classical diffusion coefficient, and V is the convection velocity representing temperature screening. The source term is assumed to be vanishingly small for the reasons discussed previously. The ion temperature and the main ion (deuteron) density profiles (calculated from the electron and impurity density profiles assuming charge neutrality) are shown in Fig. 2(b) and (c) respectively. The ion temperature is measured to be constant during

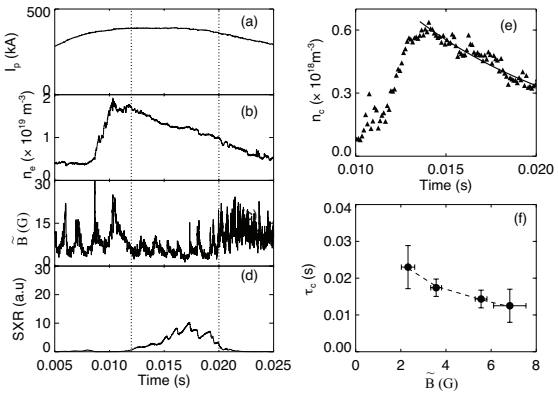

FIG. 3. [Left] Typical time evolution of impurity pellet injected discharges. (a) Plasma current, (b) line averaged electron density, (c) mean amplitude of core-resonant modes (m=1, n=7-12) and (d) soft-x-ray emission. Time window between dotted vertical lines represents duration of PPCD. [Right] (e) Time evolution of on-axis C^{+6} density showing the increase due to pellet injection and a slow decay afterward. The exponential fit to the impurity decay is also shown (solid line). (f) On-axis impurity decay time correlated with the mean amplitude of the core-resonant modes. The dotted line in figure(f) shows the empirical relationship, $\tau_c \propto \frac{1}{n_e^{0.1}\tilde{B}^{0.5}}$ (see text).

PPCD, while for simplicity the main ion density is fixed, as this does not strongly affect the impurity profile evolution. As shown in Fig. 2(a), a hollow profile of carbon is predicted to appear rapidly in ∼10 ms due to the strong temperature screening effect, and then evolves to its stationary shape in about 30-40 ms. The experimental impurity profile at the end of the PPCD period (which lasts 10-15 ms) is also shown for comparison. The experimental profile is scaled for a best fit since the initial carbon density is determined by processes in pre-PPCD conditions. The model profile agrees well with the experimental profile, both in magnitude and shape. The predicted evolution is also close to the observed evolution, most notably the relatively rapid formation of the hollow shape due to temperature screening.

Experiments performed with methane (CH_4) pellet injection provide further evidence for classical impurity ion confinement when tearing instabilities are suppressed. A pellet injector designed to make deuterium pellets [28] was straightforwardly modified to form CH_4 pellets (∼1 mm diameter, ∼2 mm long) that were injected into PPCD plasmas with a speed of ∼ 200 m/s. The time evolution of plasma parameters for a typical impurity-pellet-injected plasma is shown in Figs.3(a)-(d). The time evolution of the on-axis C^{+6} density

shows an initial increase due to pellet injection followed by a slow decay [Fig.3(e)].

A characteristic impurity confinement time τ_c is obtainable from an exponential fit to the decaying density waveform following the onset of improved confinement, as shown in Fig.3(e). Pellet injection increases the plasma density, which affects the PPCD-induced fluctuation suppression [29] and exposes sensitivity of τ_c on $\tilde{B}$, as shown in Fig.3(f). A model for classical transport analogous to that described above, except that the initial carbon density profile is assumed much more peaked (as expected for pellet injection), predicts classical (*i*.e., maximum) $\tau_c \sim$ 30-45 ms[30]. As $\tilde{B}$ decreases, τ_c approaches this classical value. The line connecting the data points scales as $\tau_c \propto \tilde{B}^{-0.5}$, with an additional weak dependence on density. For reference, particle transport in a stochastic magnetic field would be expected to scale as $\tau_c \propto \tilde{B}^{-2}$ [17]. All cases in Fig.3(f) have reduced magnetic fluctuations relative to the standard RFP case where stochastic transport is expected to be dominant, so transport that is not fully stochastic might be expected. There may be other implicit dependencies, especially the plasma temperature.

In conclusion, we present the first experimental observation of classical impurity ion confinement in a toroidal magnetized plasma. The radial profile of C^{+6} is hollow when magnetic fluctuations are suppressed. The core impurity density decays slowly in time, concurrent with an increase in impurity density in the outer region, indicating outward convection of impurity ions. The profiles agree well with classical expectations. Experiments with impurity pellet injection corroborate the observation of classical impurity ion confinement. The impurity expulsion is due to the "temperature screening effect," which has favorable implications for impurity removal in a RFP fusion reactor.

The authors would like to thank L. Lin for providing electron density profile data, S. Eilerman for providing neutral density profile data, and J. K. Anderson and M. Nornberg for useful discussions. This work is supported by the US DoE under cooperative agreement DE-FCO2-05ER54814 and by NSF-PHY0821899.

* stkumar@wisc.edu

† Currently at West Virginia University, Morgantown, WV, USA

[1] K. Miyamoto, *Plasma physics for nuclear fusion* (MIT Press, 1989).

[2] R. Dux, C. Giroud, K. Zastrow, and JET EFDA Contributors, Nucl. Fusion **44**, 260 (2004).

[3] L. Delgado-Aparicio *et al.*, Nucl. Fusion **49**, 085028 (2009).

[4] E. J. Doyle (Chair Transport Physics) *et al.*, Nuclear Fusion **47**, S18 (2007).

[5] T. S. Chen, A. Nagata, K. Sato, H. Ashida, and T. Amano, J. Phys. Soc. Jpn. **61**, 530 (1992).

[6] H. Oshiyama and S. Masamune, J. Phys. Soc. Jpn. **52**, 2041 (1983).

[7] M. Wakatani and R. Itatani, J. Phys. Soc. Jpn. **34**, 181 (1973).

[8] M. Gobbin, L. Guazzotto, S. C. Guo, I. Predebon, F. Sattin, G. Spizzo, P. Zanca, and S. Cappello, J. Plasma Fusion Res. Series **8**, 1147 (2009).

[9] J. S. Sarff, S. A. Hokin, H. Ji, S. C. Prager, and C. R. Sovinec, Phys. Rev. Lett. **72**, 3670 (1994).

[10] B. E. Chapman *et al.*, Phys. Plasmas **9**, 2061 (2002).

[11] P. Franz, L. Marrelli, P. Piovesan, B. E. Chapman, P. Martin, I. Predebon, G. Spizzo, R. B. White, and C. Xiao, Phys. Rev. Lett. **92**, 125001 (2004).

[12] R. O'Connell *et al.*, Phys. Rev. Lett. **91**, 045002 (2003).

[13] J. S. Sarff *et al.*, Plasma Phys. Control. Fusion **45**, A457 (2003).

[14] R. N. Dexter, D. W. Kerst, T. W. Lovell, S. C. Prager, and J. C. Sprott, Fusion Technol. **19**, 131 (1991).

[15] M. R. Wade, W. A. Houlberg, and L. R. Baylor, Phys. Rev. Lett. **84**, 282 (2000).

[16] M. Yoshinuma *et al.*, Nucl. Fusion **49**, 062002 (2009).

[17] A. B. Rechester and M. N. Rosenbluth, Phys. Rev. Lett. **40**, 38 (1978).

[18] J. K. Anderson *et al.*, Phys. Plasmas **12**, 056118 (2005).

[19] D. J. Den Hartog *et al.*, Rev. Sci. Instrum. **77**, 10F122 (2006).

[20] D. Craig, D. J. Den Hartog, D. A. Ennis, S. Gangadhara, and D. Holly, Rev. Sci. Instrum. **78**, 013103 (2007).

[21] S. Gangadhara, D. Craig, D. A. Ennis, and D. J. Den Hartog, Rev. Sci. Instrum. **77**, 10F109 (2006).

[22] S. T. A. Kumar, D. J. Den Hartog, R. M. Magee, G. Fiksel, and D. Craig, Plasma Phys. Control. Fusion **53**, 032001 (2011).

[23] H. P. Summers, *The Atomic Data and Analysis Structure User Manual, version 2.6*

(www.adas.ac.uk) (2004).

[24] S. P. Hirshman and D. J. Sigmar, Nucl. Fusion **21**, 1079 (1981).

[25] K. W. Wenzel and D. J. Sigmar, Nucl. Fusion **30**, 1117 (1990).

[26] V. Zhdanov, *Transport Processes in Multicomponent Plasma* (Taylor & Francis, London, 2002).

[27] S. T. A. Kumar, D. J. Den Hartog, B. E. Chapman, M. O'Mullane, M. Nornberg, D. Craig, S. Eilerman, G. Fiksel, E. Parke, and J. Reusch, Plasma Phys. Control. Fusion **54**, 012002 (2012).

[28] S. K. Combs *et al.*, Fusion Sci. Technol. **44**, 513 (2003).

[29] M. Wyman *et al.*, Nuclear Fusion **49**, 015003 (2009).

[30] As these plasmas are not as well diagnosed and profiles must be assumed, the characteristic classical connement time is more uncertain. Note that the impurity ion collision frequency is likely higher than for the non-pellet case.